# 4×20Gbit/s-40GHzOFDM based Radio over FSO transmission link incorporating hybrid wavelength division multiplexing-mode division multiplexing of LG and HG modes with enhanced detection

MEHTAB SINGH*, JYOTEESH MALHOTRA
*Department of Engineering and Technology, Guru Nanak Dev University, Regional Campus, Jalandhar, India*

The present work reports the designing and performance analysis of radio over free space optics transmission link by incorporating hybrid wavelength division multiplexing, mode division multiplexing, and orthogonal frequency division multiplexing techniques. Four independent information signals each carrying 20Gbit/s-40GHz data are transmitted using distinct Laguerre Gaussian (LG) modes and Hermite Gaussian (HG) modes (LG02, LG03, HG02, and HG03)over different atmospheric conditions. The proposed link performance is investigated under the impact of geometric losses and for varying climate conditions viz. clear, light fog, moderate fog, and heavy fog. Also, the impact of increasing size of optical beam (beam divergence) on the proposed link performance has been numerically investigated. The modal decomposition of different channels at the receiver terminal is also evaluated. Furthermore, to increase the maximum link range of the proposed link under adverse climate conditions, we have deployed a Square root module at the receiver end and the efficacy of the proposed detection technique is demonstrated.

(Received December 30, 2018; accepted June 16, 2020)

*Keywords:* WDM, MDM, OFDM, RoFSO, Atmospheric turbulences, Square root module

## 1. Introduction

The ever-growing demand for higher channel bandwidth as a result of massive rise in the utilization of high bandwidth expending services has challenged the International Telecommunication Union (ITU) to effectively and reliably allocate limited radio frequency (RF) spectrum to meet the demands of the end users [1]. Radio over free space optics (RoFSO) technology has the potential for last-mile data transmission along with many other merits such as no licensing necessity, enormous channel capacity, large bandwidth, secure networks, low cost, lightweight, and easy deployment [2]. Such virtue qualifies RoFSO links as a promising candidate in the next-generation wireless communication networks [3]. RoFSO links allow an ideal integration of RF networks and optical networks [4]. However, external climate conditions, increasing size of optical beam as it propagates through atmosphere (beam divergence), scintillation, and atmospheric turbulence result in the loss of optical beam signal power which limits the performance of the link. In orthogonal frequency division multiplexing (OFDM), the data is transmitted over a number of sub-carriers which are perpendicular to each other and are spaced apart in the frequency domain at precise frequencies [5]. The orthogonality is achieved using Fast Fourier Transform algorithm. The hybridization of OFDM technique in RoFSO links can effectively reduce the adverse effect of multipath fading and enhance the quality of the received signal [6]. Owing to its high power and spectral efficiency, OFDM can be used to enhance the system flexibility along with increased coverage area without increasing the complexity and cost of the system. The performance of OFDM based FSO links under the effect of atmospheric turbulence has been demonstrated in [7]. A 300 Mbit/s OFDM based FSO link over a link distance of 1.87 km has been experimentally demonstrated in [8].

The capacity of RoFSO links can be enhanced by multiplexing in intensity [9], wavelength [10-11], and phase dimensions [12]. On the other hand, mode division multiplexing (MDM) is an emerging multiplexing technique in which multiple independent information carrying signals are transmitted using different spatial modes. The work in [13-15] report the use of optical signal processing techniques to generate different spatial modes of a single laser beam. Spatial light modulator (SLM) has been investigated in [16, 17] for generating multiple spatial laser modes. Here in [18] the authors report the application of single mode fiber for spatial multiplexing. Similarly in [19] photonic crystal fiber has been deployed for MDM. The authors in [20] report the generation of highly pure and power-efficient 7 orbital angular multiplexing (OAM) modes using a ring fiber in MDM systems. The authors have reported a purity of 99 % for each of the generated mode. The feasibility of the use of solid core vortex fiber for implementing MDM in optical fiber communication links is discussed in [21]. The experimental demonstration of a power-effective multimode information transmission for short reach optical links in access networks over a 200 m few mode fiber by

incorporating OAM of two beams with corresponding topical charge of $l = 0$ and $l = 1$ has been investigated in [22]. The authors in [23] discuss the experimental demonstration of fabrication of hollow air core optical fiber that can support up to 16 OAM beams for MDM application in optical communication links. The authors in [24] discuss a 2×10 Gbit/s transmission over 1 km ring core fiber by incorporating MDM of OAM modes and using SLM for all optical mode multiplexing and de-multiplexing. The use of OAM fiber amplifier in a hybrid OAM-WDM based optical fiber link to achieve a target bit error rate of $2\times 10^{-3}$ with 1.8 dB optical-signal to noise ratio penalty for all spatial channels has been demonstrated in [25]. The fabrication of phase-only diffraction optical devices using high-resolution electron beam in order to achieve MDM of OAM beam in optical fiber links with less than -12 dB crosstalk has been demonstrated in [26]. The experimental transmission of 3×10 Gbps information using on-off keying modulation and 2×100 Gbps information using dual polarization-quadrature phase shift keying modulation in optical fiber links using MDM of OAM beams for realizing 5G networks has been reported in [27]. The experimental demonstration of OAM distributed RAMAN amplifier over 18 km multimode fiber using MDM of 2 OAM beams and WDM of 16 wavelength channels has been reported in [28]. The fabrication of all optical mode coupler with negligible mode crosstalk in a 16-quadrature amplitude modulation based optical fiber link incorporating MDM of OAM beams has been reported in [29]. Similarly, the works in [30-36] discuss the application of MDM in FSO links for high-reach optical wireless information transmission links.

In this work, we demonstrate hybrid WDM-MDM-OFDM of Hermite Gaussian (HG) modes and Laguerre Gaussian (LG) modes for transmitting four independent information signals each carrying 20Gbit/s-40GHz data over a RoFSO link under the effect of different atmospheric conditions. Section 2 describes the link design and the simulation results are illustrated in Section 3. The conclusions are discussed in Section 4.

## 2. Link design

The proposed link design for OFDM based RoFSO link incorporating hybrid WDM-MDM is shown in Fig. 1. The proposed work is performed using Opti system software.

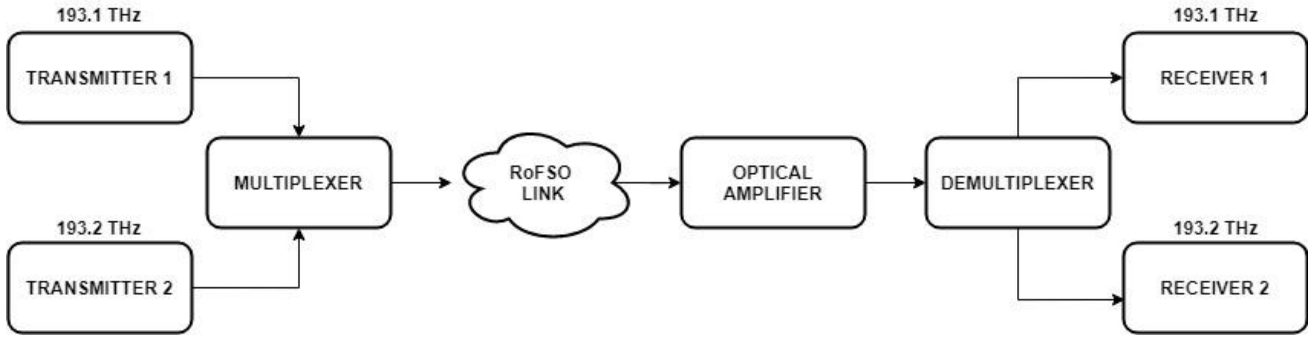


*Fig. 1. (a) Proposed 2-wavelength channel WDM-MDM based OFDM-RoFSO transmission link*

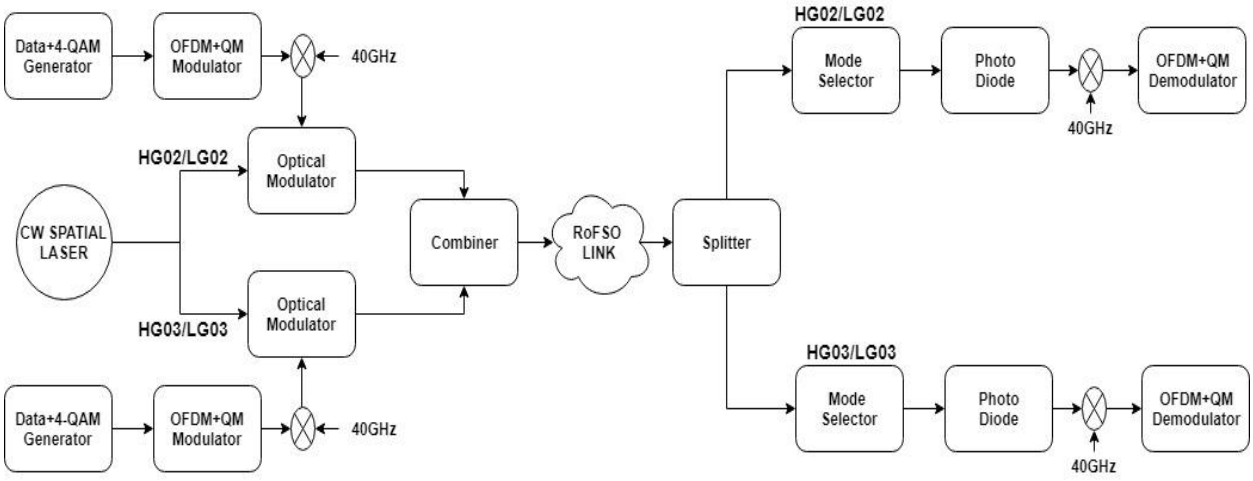


*Fig. 1. (b) Schematic of each sub-channel in the proposed link*

Four distinct Quadrature Amplitude Modulation (QAM) signals having 20Gbit/s-40GHz data are transported over spatial modes (HG02, HG03, LG02, and LG03) as shown in Fig. 2. In this work, we have demonstrated the use of both LG and HG modes to exploit the increase in the degree of freedom for multiplexing. The HG modes are mathematically described as [37]:

$$\varphi_{m,n}(r,\emptyset) = H_m\left(\frac{\sqrt{2}x}{\omega_{0,x}}\right)\exp\left(-\frac{x^2}{\omega_{ox}^2}\right)\exp\left(j\frac{\pi x^2}{\lambda R_{ox}}\right) \times H_n\left(\frac{\sqrt{2}y}{w_{o,y}}\right)\exp\left(-\frac{y^2}{w_{oy}^2}\right)\left(j\frac{\pi y^2}{\lambda R_{oy}}\right) \quad (1)$$

whereas the LG modes are mathematically described as [37]:

$$\varphi_{m,n}(r,\emptyset) = \left(\frac{2r^2}{w_o^2}\right)^{|n/2|} L_m^n\left(\frac{2r^2}{w_0^2}\right)\exp\left(\frac{r^2}{w_0^2}\right)\exp\left(j\frac{\pi r^2}{\lambda R_0}\right)\begin{Bmatrix} sin(|n|\emptyset), n \geq 0 \\ cos(|n|\emptyset), n < 0 \end{Bmatrix} \quad (2)$$

Where mode dependency of X-polarization axis is denoted by m, mode dependency on Y-axis is denoted by n, the beam curvature radius is denoted by R, the beam spot size is denoted by $w_o$, $L_m^n$ represents the Laguerre polynomial and $H_m$ *and* $H_n$ represent Hermite polynomials.

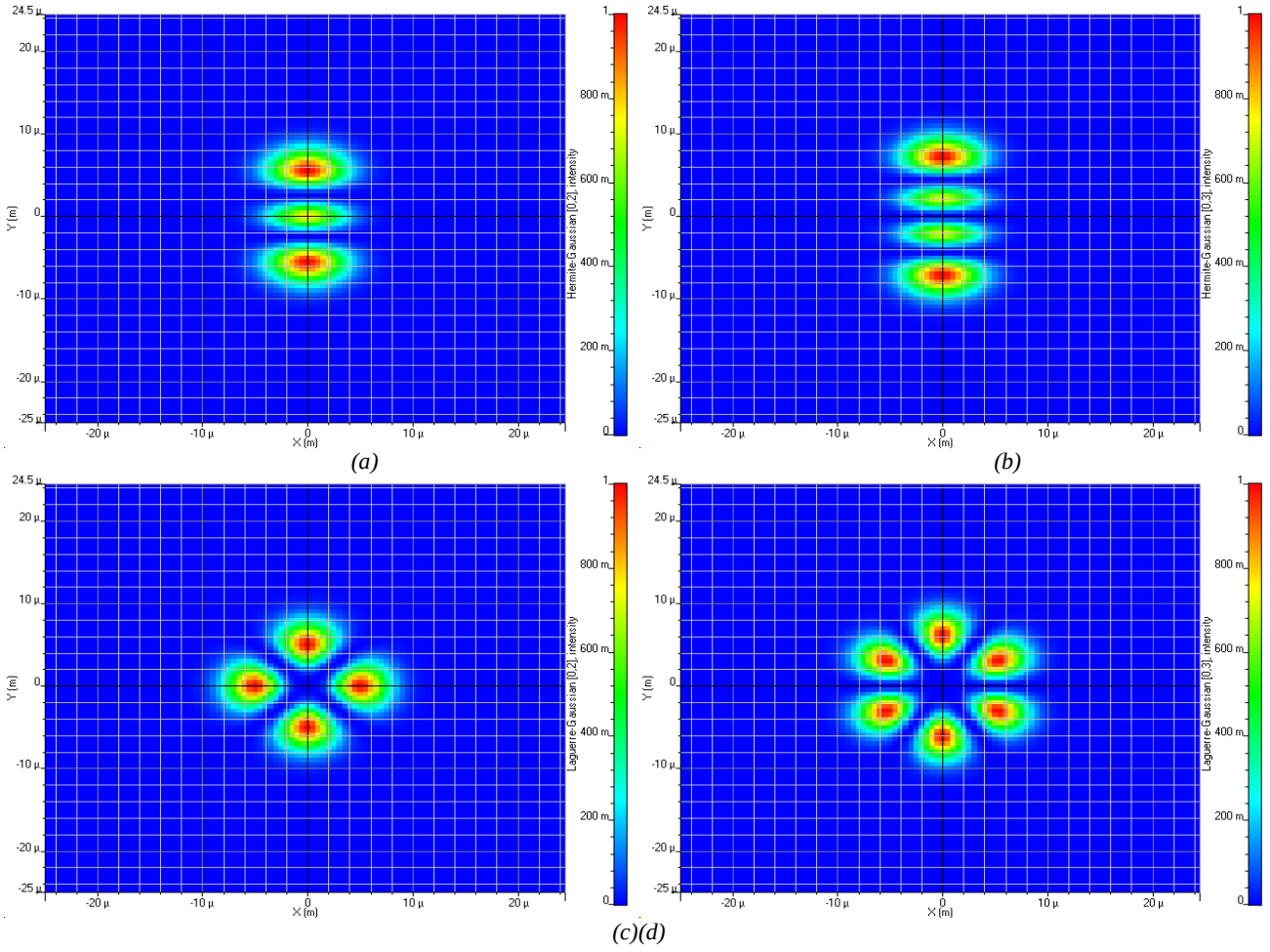


*Fig. 2. Excited modes (a) HG02 mode (b) HG03 mode (c) LG02 mode (d) LG03 mode (color online)*

20 Gbit/s binary data transmitting 2-bits/symbol is generated using QAM generator. This data is OFDM modulated over 512 orthogonal carriers using 1024 IFFT algorithm which is further mixed with a 7.5 GHz signal from Quadrature modulator (QM). A 40GHz RF signal is mixed with this signal using a mixer. The information signal is transported to atmospheric channel using HG02 and HG03 modes of 193.1 THz frequency channel and LG02 and LG03 modes of 193.2 THz frequency channel. The link equation can be expressed as [38]:

$$P_{Received} = P_{Transmitted}\left(\frac{d_R^2}{(d_T + \theta Z)^2}\right)10^{-\sigma Z/10} \quad (3)$$

Where receiver antenna diameter (10 cm) and transmitter antenna diameter (10 cm) are denoted by $d_R$ and $d_T$ respectively, the angle of divergence of beam (0.25 mrad) is denoted by $\theta$, the FSO range is denoted by Z, and specific attenuation coefficient is denoted by $\sigma$. In our proposed study, the specific attenuation for clear weather is taken as 0.155 dB/km whereas for light, moderate, and heavy fog is taken as 9, 12, and 16 dB/km respectively [39]. At the receiver terminal, a non-interferometric modal decomposition based mode selector is used for mode separation [40]. The information carrying optical beam is converted to electric signal using a spatial PIN photodiode. QAM demodulator is used for the demodulation of the electric signal followed by data recovery using OFDM and QM decoder.

The specific attenuation due to fog can be determined using the following equation [41]:

$$\beta_{fog}(\lambda) = \frac{3.91}{V}\left(\frac{\lambda}{550}\right)^{-p} \tag{4}$$

where V (km) represents range of visibility, $\lambda\ (nm)$ is the wavelength and $p$ is the distribution coefficient of scattering and can be determined by Kim model as [42]:

$$p = \begin{cases} 1.6 & V > 50 \\ 1.3 & 6 < V < 50 \\ 0.16V + 0.34 & 1 < V < 6 \\ V - 0.5 & 0.5 < V < 1 \\ 0 & V < 0.5 \end{cases} \tag{5}$$

and Kruse model as [43]:

$$p = \begin{cases} 1.6 & V > 50 \\ 1.3 & 6 < V < 50 \\ 0.585V^{\frac{1}{3}} & V < 6 \end{cases} \tag{6}$$

Using the above equations, the attenuation for light fog, moderate fog, and heavy fog conditions are calculated to be9 dB/km, 12 dB/km, and 16 dB/km respectively. The geometric losses $(A_{Geo})$ with increasing FSO range are illustrated in Fig. 3 which can be approximated using the equation [44]:

$$A_{Geo} = 10log_{10}\left[\frac{4A_{RX}}{\pi(\theta Z)^2}\right]\text{dB} \tag{7}$$

where area of the receiver surface is denoted by $A_{RX}$, angle of divergence of beam in mrad by $\theta$, and FSO range in km by Z .

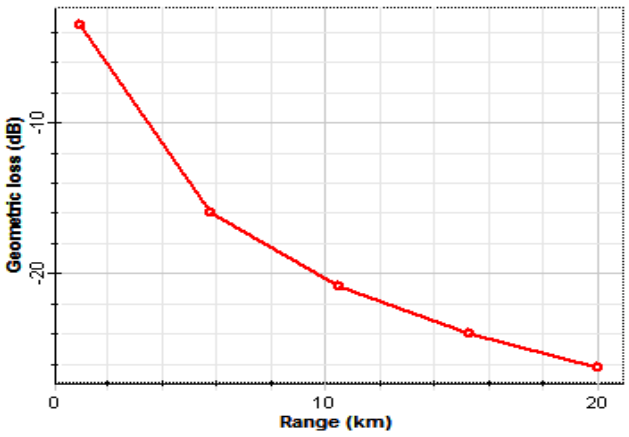


*Fig. 3. Geometric loss v/s FSO link range*

## 3. Results and discussions

This section presents the results of the simulative analysis of the proposed link. Also, an improved performance of the proposed link using an enhanced detection technique is demonstrated in the latter part of this section.

### 3.1. Performance analysis of the proposed OFDM based RoFSO transmission link

Fig. 4 (a) and (b) illustrates the signal to noise ratio (SNR) and total power of the information signal at the surface of photodetector using the proposed link for increasing FSO range. The results in Fig. 4 (a) show that the SNR is calculated as 42.32, 32.66, 27.49, 23.59, and 20.19 dB for HG02 mode; 41.84, 32.17, 26.98, 23.04, and 19.58 dB for HG03 mode; 42.19, 32.53, 27.36, 23.44, and 20.03 dB for LG02 mode; and 38.73, 28.98, 23.56, 19.24, and 15.32 dB for LG03 mode at FSO range of 2, 6.5, 11, 15.5, and 20 km respectively. Alternatively, Fig. 4 (b) shows that the total power at the photodetector is calculated as -20.46, -39.72, -49.70, -56.76, and -62.31 dBm for HG02 mode; -21.41, -40.68, -50.65, -57.70, and -63.22 dBm for HG03 mode; -20.71, -39.98, -49.96, -57.01, and -62.55 dBm for LG02 mode; and -27.64, -46.89, -56.81, -63.73, and -68.99 dBm for LG03 mode at FSO range of 2, 6.5, 11, 15.5, and 20 km respectively. The results in Fig. 4 (a) and (b) show that with increasing FSO range, the performance of the link in terms of SNR and power of the information signal at the photodetector surface degrades for all channels. This is because with increasing FSO range, the information carrying optical beam is attenuated due to atmospheric attenuation which reduces the optical power and SNR at the receiver terminal and reduces the maximum FSO range. Also, it is observed that all the spatial channels are transported faithfully at 20 km FSO range with sufficient SNR and total power for reliable information transmission. Fig. 5 illustrates the RF power collected at the photodetector surface for all the spatial channels at FSO range of 20 km. Here, it is seen

that highest RF power is observed in the case of HG02 mode, preceding HG03 mode, LG02 mode, and LG03 mode. High RF power guarantees reliable recovery of the transmitted information message at the receiver terminal. Similarly, Fig. 6 illustrates the constellation graphs of the recovered information channels at FSO range of 20 km. Here, it is observed that for all channels, the constellation symbols are clear having distinct and symmetric distribution which shows reliable interception of the information message. Further, the results discussed in Fig. 4-6 show that HG02 mode shows superior performance in terms of SNR, optical power, RF power and constellation graph at the receiver preceding HG03 mode, LG02 mode, and LG03 mode. Hence, HG02 mode demonstrates more robust performance against FSO channel effects and LG03 mode demonstrates worst performance.

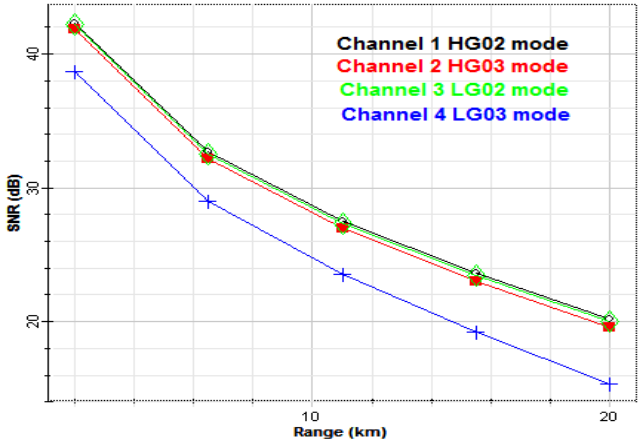


*(a)*

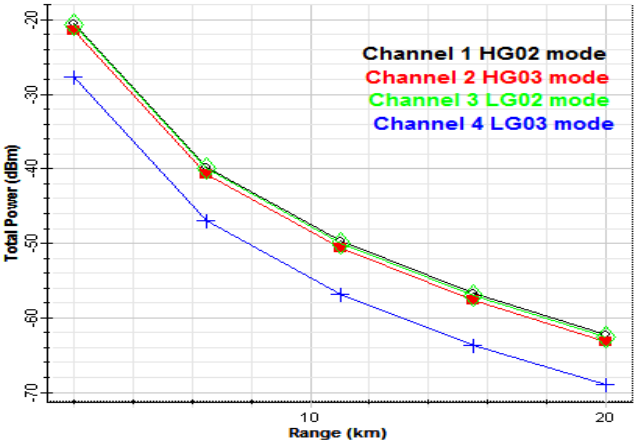


*(b)*

*Fig. 4. (a) SNR (b) Received power v/s FSO range under clear weather conditions (color online)*

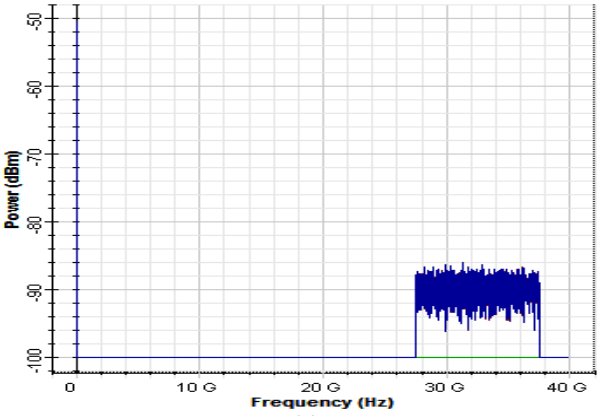


*(a)*

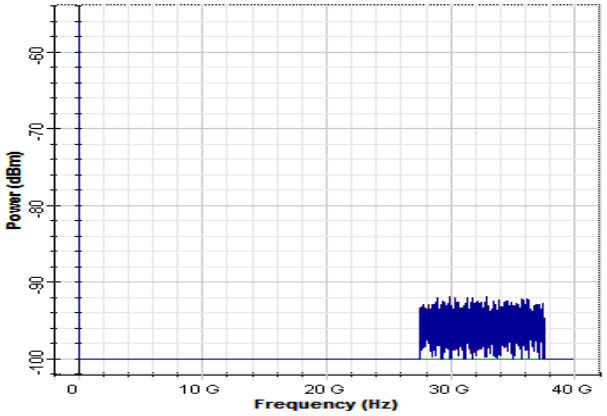


*(b)*

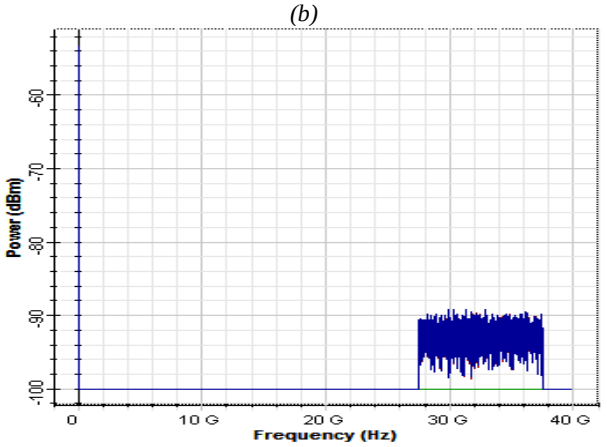


*(c)*

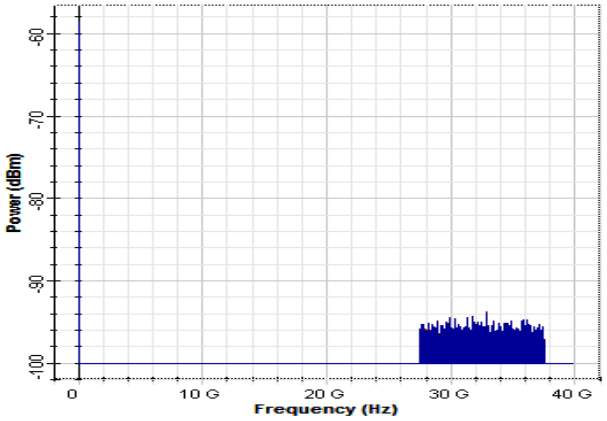


*(d)*

*Fig. 5. RF power for (a) HG02 (b) HG03 (c) LG02 (d) LG03 at 20 km FSO range (color online)*

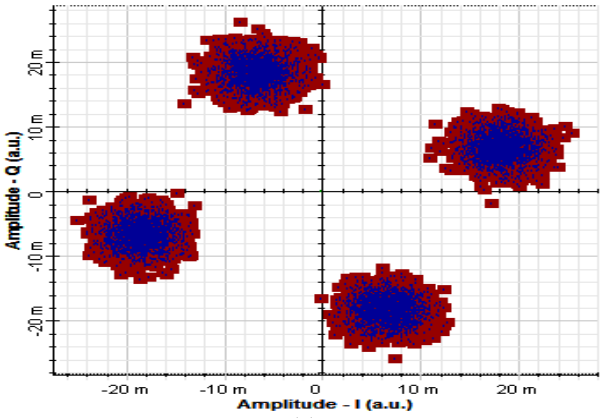


*(a)*

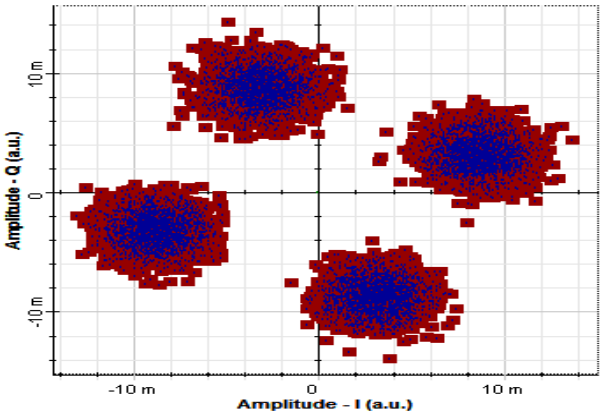


*(b)*

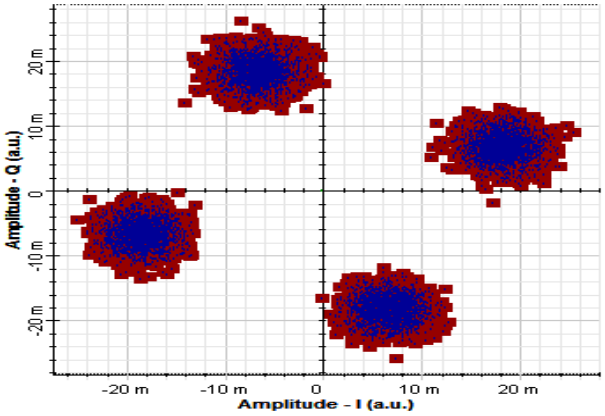


*(c)*

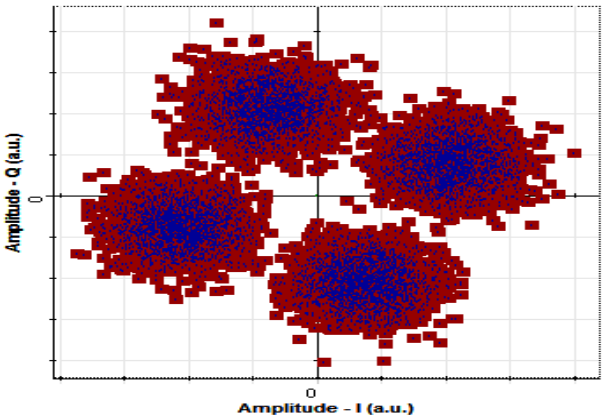


*(d)*

*Fig. 6. Constellation graph for (a) HG02 (b) HG03 (c) LG02 (d) LG03 at 20 km FSO range (color online)*

As the information carrying optical beam propagates through the atmospheric channel, it gets diverged due to diffraction phenomenon. Since, the receiver telescope has a limited field of view, only a portion of the optical beam power is collected at the receiver antenna whereas the rest of the optical power is lost to the surroundings. This is referred as beam divergence or geometric loss. Here, we have investigated the impact of geometric loss on the proposed link performance. Fig. 7 illustrates the link performance for all spatial channels with angle of divergence increasing from 0.2 mrad to 1.0 mrad at FSO range of 10 km. The results show that increasing angle of divergence degrades the quality of the received signal which should be expected as increasing angle of divergence means more loss of optical signal power to the surroundings. The performance comparison of different channels as a function of increasing angle of divergence is presented in Table1. From results presented in Table1, it can be seen that the SNR and received power is highest for HG02 channel which is most robust to multipath fading and is lowest for LG03 channel which is most prone to fading effects. From the results in Fig. 7 and Table 1, it is observed that all the channels are reliably transported up to a FSO range of 10 km with angle of divergence of 0.5 mrad. Beyond that, the signal performance degrades and the message signal cannot be intercepted without errors.

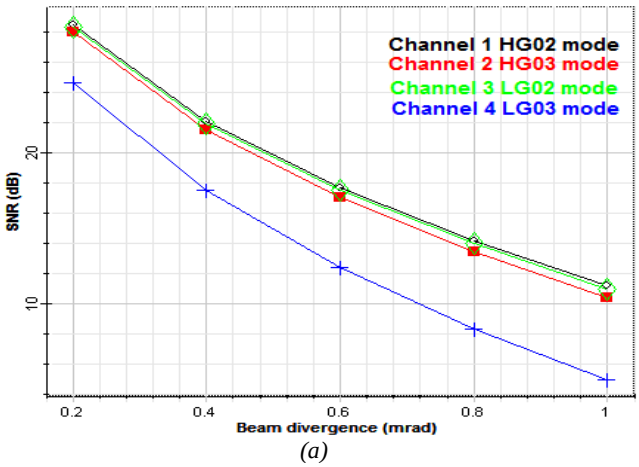


*(a)*

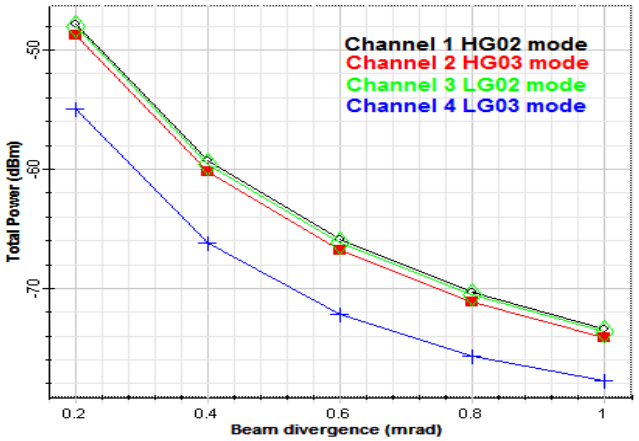


*(b)*

*Fig. 7. (a) SNR (b) Received power v/s Beam divergence angle (color online)*

*Table 1. Performance comparison of different channels with increasing beam divergence angles*

| Beam divergence angle (mrad) | Channel 1 (HG02 mode) | | Channel 2 (HG03 mode) | | Channel 3 (LG02 mode) | | Channel 4 (LG03 mode) | |
|---|---|---|---|---|---|---|---|---|
| | SNR (dB) | Power (dBm) | SNR (dB) | Power (dBm) | SNR (dB) | Power (dBm) | SNR (dB) | Power (dBm) |
| 0.2 | 28.49 | -47.83 | 27.98 | -48.78 | 28.35 | -48.08 | 24.62 | -54.95 |
| 0.4 | 22.08 | -59.30 | 21.51 | -60.23 | 21.92 | -59.55 | 17.51 | -66.17 |
| 0.6 | 17.71 | -65.91 | 17.05 | -66.80 | 17.53 | -66.15 | 12.43 | -72.21 |
| 0.8 | 14.18 | -70.34 | 13.45 | -71.14 | 13.98 | -70.55 | 8.36 | -75.72 |
| 1.0 | 11.17 | -73.43 | 10.39 | -74.13 | 10.96 | -74.62 | 4.98 | -77.74 |

The spatial channels at the receiver terminal are decomposed into linear polarized (LP) modes using a mode filter as illustrated in Fig. 8. Here, it is observed that in the case of HG02 mode, highest power is transferred to LP [2,1] preceding LP [0,2], LP [0,3], LP [2, 2], and LP [0, 1]. Similarly, in the case of HG03 mode, highest power is transferred to LP [1, 2] preceding LP [3, 1], LP [1, 3], LP [1, 1], and LP [3, 2]. Also, in the case of LG02 mode, highest power is transferred to LP [2, 1] preceding LP [2, 2], LP [2, 3], and LP [2, 4]. In the case of LG03 mode, the highest power is transferred to LP [3, 1] preceding LP [3, 2], LP [1, 2], and LP [1, 3].

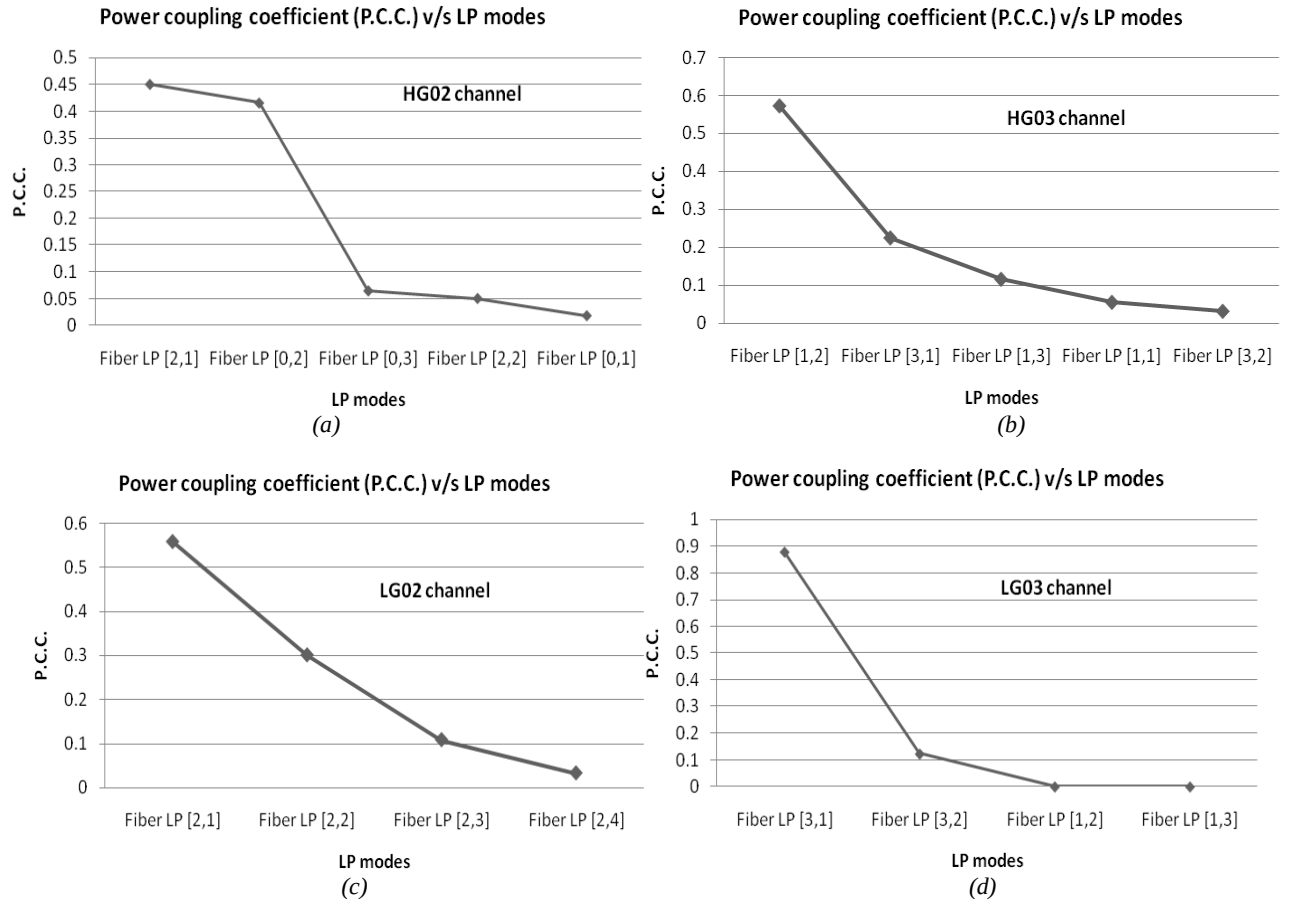


*Fig. 8. Modal decomposition v/s Fiber LP modes for (a) HG02 (b) HG03 (c) LG02 (d) LG03*

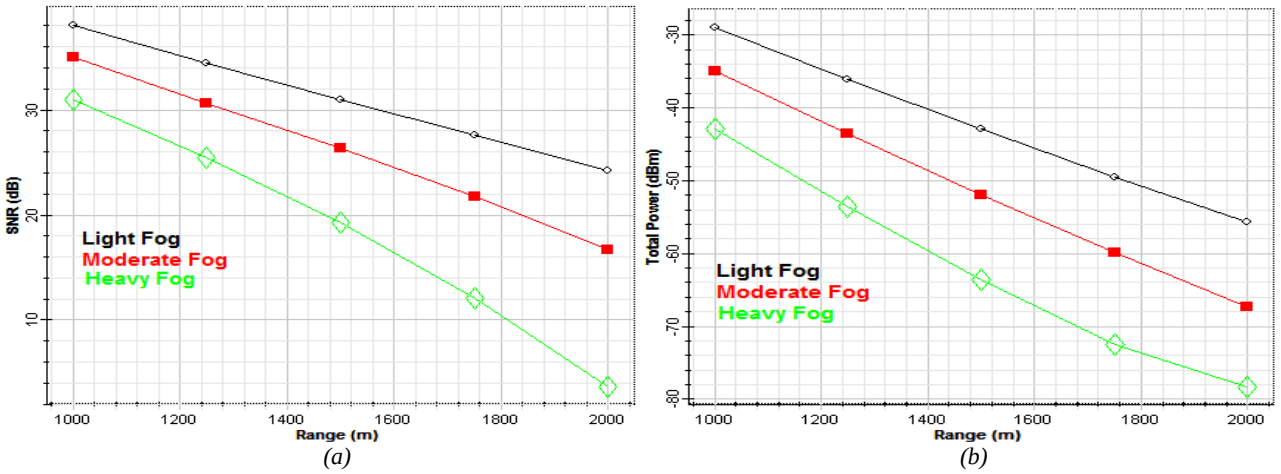


*(a)* *(b)*

*Fig. 9. (a) SNR (b) Received power v/s FSO Range for varying climate conditions (color online)*

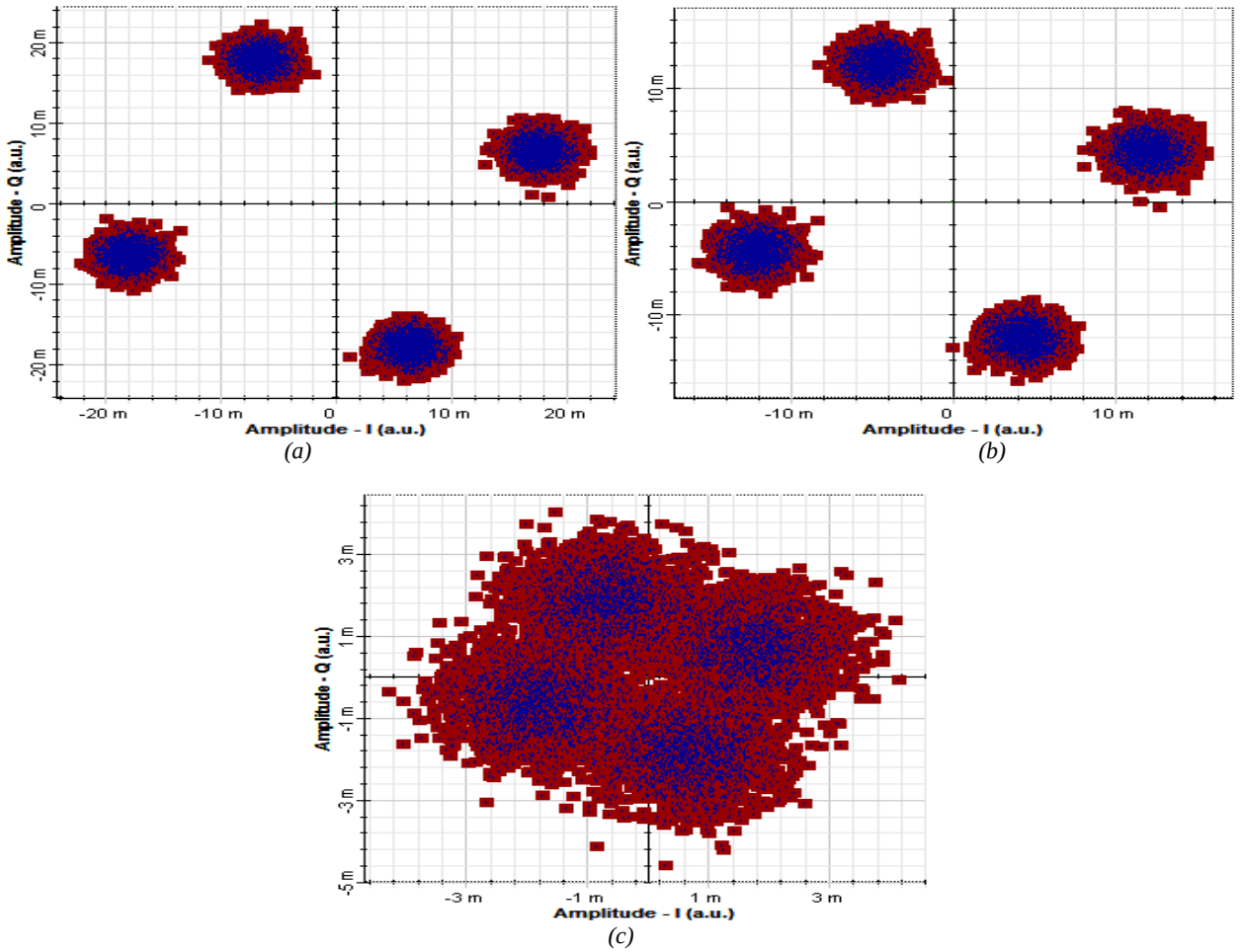


*(a)* *(b)* *(c)*

*Fig. 10. Constellation graph for (a) Low (b) Moderate (c) Heavy Fog at 2000 m FSO range (color online)*

One of the most important climate condition which degrades the performance of FSO link is fog weather, since the size of fog particle is comparable to the operating wavelength deployed in FSO links. So, we have investigated the link performance under the impact of fog weather as illustrated in Fig. 9 (a) and (b). Here, only

HG03 mode is considered since all the other spatial channels perform similarly. The graphs in Fig. 9 (a) report that the SNR is calculated as 38.07, 34.47, 31.02, 27.62, and 24.18 dB under light fog; 35.06, 30.67, 26.32, 21.77, 16.71 dB under moderate fog; and 31.02, 25.40, 19.31, 12.09, and 3.61 dB under heavy fog at FSO range of 1000, 1250, 1500, 1750, and 2000 m respectively. Similarly, the graphs in Fig. 9 (b) report that the power at the receiver is calculated as -28.96, -36.13, -42.94, -49.46, and -55.72 dBm under light fog; -34.96, -43.62, -51.89, -59.81, and -67.25 dBm under moderate fog; and -42.94, -53.55, -63.62, -72.55, and -78.34 dBm under heavy fog at FSO range of 1000, 1250, 1500, 1750, 2000 m respectively. From the results in Fig. 9, it is seen that the received signal degrades more as the climate changes from light to heavy fog. This is because, as the climate changes from light to heavy fog, more amount of optical signal power loss per unit distance occurs since the atmospheric attenuation is higher for heavy fog, preceding moderate fog, and low fog. The maximum FSO range achieved using the proposed link from the investigations illustrated in Fig. 9 is computed as 2000, 1800, and 1500 m under light, moderate, and heavy fog respectively. Further, in Fig. 10 we have presented the constellation graphs of the received signal at 2000 m FSO range for varying levels of fog climate. Here, it is observed that most signal distortion is seen in the case of heavy fog whereas least signal distortion is in the case of light fog. This is because more optical power loss occurs in the case of heavy fog due to higher specific attenuation coefficient whereas less optical power loss is there in the case of light fog owing to lower specific attenuation coefficient.

### 3.2. Improved performance analysis of the proposed link using Square root module (SRm)

The temporal dispersion in RoFSO links posses limitation on the data transmission rates thus decreases the bandwidth of the channel. The scattering of the signal due to different atmospheric conditions results in temporal dispersion of the information signal transmitted due to multiple propagation paths thus leading to inter symbolic interference (ISI). The quadratic transfer function of the PIN photodiode used at the receiver terminal converts this linear distortion into a non-linear distortion and degrades the quality of the received signal. Here, for compensating the non-linearity of PIN photodiode we propose a SRm at the receiver. The practical implementation of SRm deploying Schottky diode is discussed in [45].

Here, we investigate the efficacy of the proposed detection by comparing the proposed link performance under adverse heavy fog conditions by deploying only PIN photodiode and PIN photodiode followed by SRm as discussed in Fig. 11. From Fig. 11, it is observed that the SNR reduces from 50.69 dB to 5.23 dB in the link range of 200 m to 2000 m without using SRm. Alternatively, SNR reduces from 52.63 dB to 48.86 dB in the link range of 200 m to 2000 m with the use of SRm. Further, it can also be observed that total power of the received signal reduces from 18.30 dBm to -61.32 dBm in the link range of 200 m to 2000 m without using SRm whereas the total power reduces from 23.27 dBm to -16.57 dBm in the link range of 200 m to 2000 m with the use of SRm. This indicates that there is an effective improvement in SNR and received power in the proposed link by deploying SRm which will further help in increasing the RoFSO transmission link range. For further clarity, Fig. 12 demonstrates performance comparison in terms of the constellation graphs of the received signal at FSO range of 2000 m.

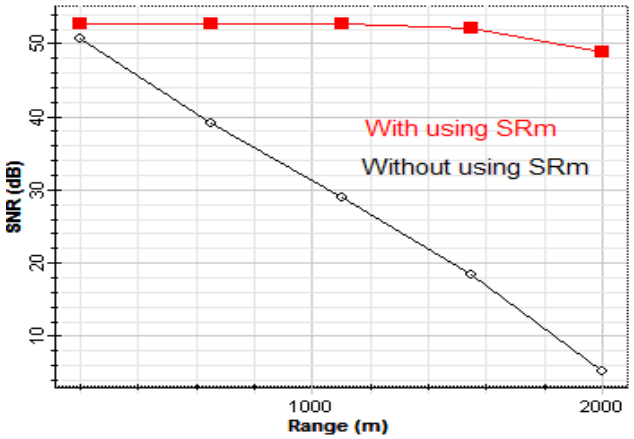


*(a)*

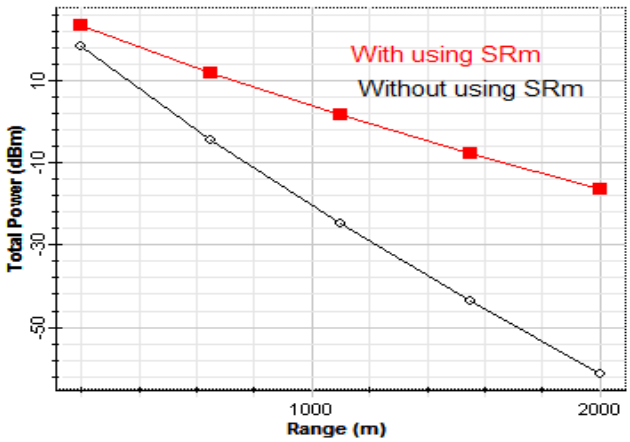


*(b)*

*Fig. 11. Performance comparison in terms of (a) SNR (b) Total power v/s FSO Range (color online)*

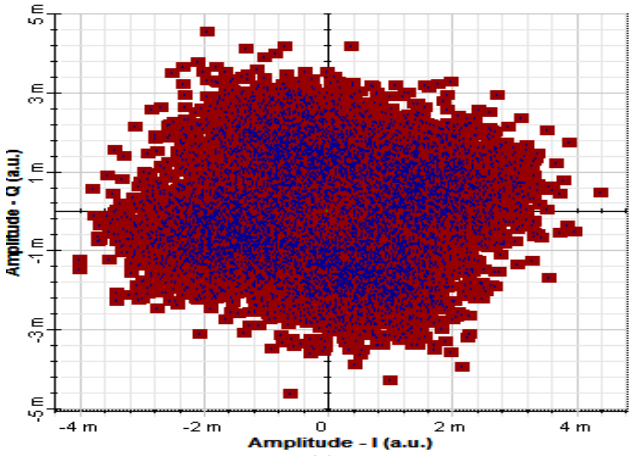


*(a)*

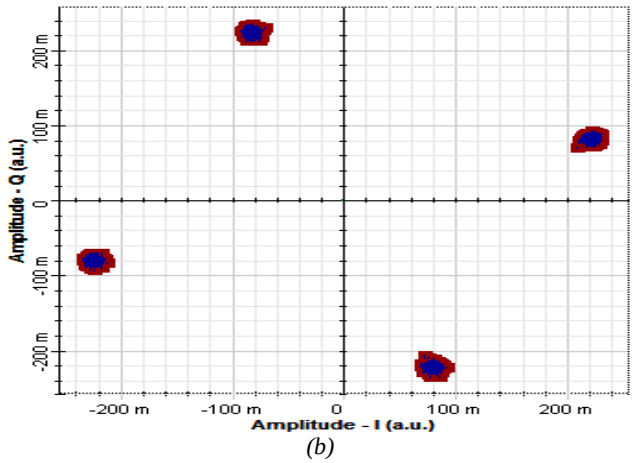


*(b)*

*Fig. 12. Constellation graphs at 2000 m FSO range (a) without SRm (b) with SRm (color online)*

## 4. Conclusion

The reported work discusses the designing of a novel WDM-MDM-OFDM based RoFSO link using distinct HG and LG mode for 80Gbit/s-160GHz transmission. The results presented show that the maximum achievable FSO range under clear weather using the proposed system is 20 km which reduces to 2000 m, 1800 m, and 1500 m under light fog, moderate fog, and heavy fog conditions respectively. Also, an enhanced performance using an SRm at the receiver terminal has been discussed. From the results presented, it can be concluded that the performance of the system is significantly enhanced by deploying the proposed enhanced detection technique which can be used for further link reach enhancement.

## References

[1] M. A. Khalighi, M. Uysal, IEEE Communications Surveys & Tutorials **16**(4), 2231 (2014).
[2] A. Mahdy, J. S. Deogun, Proceedings of IEEE Wireless Communications and Networking Conference **4**, 2399(2004).
[3] G. Nykolak, P. F. Szajowski, G. Tourgee, H. Presby, Electronic Letters **35**(7), 578 (1999).
[4] S. A. Al-Gailani, A. B. Mohammad, R. Q. Shaddad, Proceedings of IEEE 3rd International Conference on Photonics 121 (2012).
[5] A. Ramezani, M. R. Noroozi, M. Aghababaee, International Journal of Engineering and Advanced Technology **4**(1), 46 (2014).
[6] Jitendra Singh, Naresh Kumar, Optik - International Journal of Light and Electron Optics **124**(20), 4651 (2013).
[7] S. Attri, C. Narula, S. Kumar, Proc. of International Conference on Intelligent Communication, Control, Devices **479**, 167 (2012).
[8] A. Mostafa, S. Hranilovic, IEEE Photonics Technology Letters **24**, 8, 709 (2012).
[9] A. Kanno, K. Inagaki, I. Morohashi, T. KuriI. Hasako, Opt. Express **19**, B56 (2011).
[10] H. Zhou, S. Mao, P. Agarwal, Wireless Communication and Networking Conference (WCNC), IEEE **2014**, 2677 (2014).
[11] N. Kumar, A. K. Sharma, V. Kapoor, J. Opt. Commun. **35**(2), 151 (2014).
[12] C. B. Naila, K. Walkamori, M. Matsumoto, Opt. Eng. **50**, 105006 (2011).
[13] S. Randel, R. Ryf, A. Sierra, P. J. Winzer, A. H. Gnauck, C. A. Bolle, R. J. Essiambre et al., In proceedings to Optical Fiber Communication Conference and Exposition (OFC/NFOEC), (2011).
[14] A. Amphawan, O. Dominic, Proceedings of Photonics (ICP), 2010 International Conference (IEEE, Langkawi, 2010).
[15] A. Amphawan, V. Mishrab, K. Nisaran, B. Nedniyomc, J. Mod. Optic. **59**, 1745 (2012).
[16] A. Amphawan, Opt. Express **19**, 23085 (2011).
[17] A. Amphawan, J. Mod. Optic. **59**, 460 (2012).
[18] Y. Jung, R. Chen, R. Ismaeel, G. Brambilla, S. U. Alam, I. P. Giles, D. J. Richardson, Opt. Express **21**, 24326 (2013).
[19] A. Amphawan, N. Benjaporn, M. A. S. Nashwan, J. Mod. Optic. **60**(20), 1675 (2014).
[20] Y. Yan, J. Yang, Y. Yue, R. Mohammad, H. Huang, N. Ahmad, L. Zhang, J. Wang, S. Dolinar, M. Tur, A. Willner, Proc. of Conference on Lasers and Electro-Optics 1, (2012).
[21] S. Golowich, N. Bozinovic, P. Kristensen, P. Gregg, S. Ramachandran, Proc. of IEEE Photonics Society Summer Topical Meeting Series, Waikoloa, 109 (2013).
[22] P. Martelli, P. Boffi, A. Gatto, M. Martinelli, Proc. of 15th International Conference on Transparent Optical Networks, 1 (2013).
[23] C. Brunet, B. Ung, Y. Messaddeq, S. LaRochelle, E. Bernier, L. A. Rusch, Proc. of Optical Fiber Communications Conference and Exhibition OFC, 1 (2014).
[24] F. Feng, X. Jin, D. O'Brien, F. P. Payne, T. D. Wilkinson, Proc. of Optical Fiber Communications Conference and Exhibition (OFC), 1 (2017).

[25] J. Liu, H. Wang, S. Chen, S. Zheng, L. Zhu, A. Wang, N. Zhou, S. Li, L. Shen, C. Du, Q. Mo, J. Wang, Proc. of Optical Fiber Communications Conference and Exhibition (OFC), 1 (2017).
[26] G. Ruffato, M. Massari, E. Gazzola, G. Parisi, F. Romanato, Proc. of 19th Italian National Conference on Photonic Technologies (Fotonica 2017), 1 (2017).
[27] L. A. Rusch, M. Rad, K. Allahverdyan, I. Fazal, E. Bernier, IEEE Communications Magazine **56**(2), 219 (2018).
[28] L. Zhu, J. Li, G. Zhu, L. Wang, C. Cai, A. Wang, S. Li, M. Tang, Z. He, S. Yu, C. Du, W. Luo, J. Liu, J. Du, J. Wang, Proc. of Optical Fiber Communications Conference and Exposition (OFC), 1 (2018).
[29] Y. Luo, W. Zhou, L. Wang, A. Wang, J. Wang, Proc. of Optical Fiber Communications Conference and Exposition (OFC), 1, (2018).
[30] Sushank Chaudhary, Angela Amphawan, International Journal of Electronics Letters, **7**, 304 (2018).
[31] Sushank Chaudhary, Xuan Tang, Xian Wei, AEU - International Journal of Electronics and Communications **93**, 208 (2018).
[32] Sushank Chaudhary, Angela Amphawan, Photonic Network Communications **36**, 263 (2018).
[33] Sushank Chaudhary, Angela Amphawan, Laser Physics **28**, 1 (2018).
[34] Sushank Chaudhary, Angela Amphawan, Photonic Network Communications **35**, 374 (2018).
[35] Sushank Chaudhary, Angela Amphawan, Optical Engineering. **56**, 1 (2017).
[36] Himali Sarangal, Amarpal Singh, Jyoteesh Malhotra, Sushank Chaudhary, Optical and Quantum Electronics. **49**, 184 (2017).
[37] A. Ghatak, K. Thyagarajan, "An introduction to Fiber Optics", Cambridge University Press, Cambridge (1998).
[38] D. R. Kolev, K. Wakamori, M. Matsumoto, J. Lightwave Technol. **30**, 3727 (2012).
[39] H. Sarangal, A. Singh, J. Malhotra, S. Chaudhary, Opt. Quant. Electron. **49**, 184 (2017).
[40] L. Pan, C. Ding, H. Wang, Opt. Express **22**, 11677 (2014).
[41] L. C. Andrews, R. L. Phillips, "Laser Beam Propagation Through Random Media" (2nd edition, SPIE Press Book, Bellingham WA, 2005).
[42] I. Kim, B. Mcarthur, E. Korevaar, Proc. of SPIE Optical Wireless Communication **6303**, 1 (2006).
[43] P.W. Kruse, L. D. McGlauchlin, R. B. McQuistan, "Elements of infrared technology: Generation, transmission, and detection", Wiley, 1962.
[44] Recommendation ITU-R, P.1814, May 2—7.
[45] J. Prat, A. Napoli, J. M. Gene, M. Omella, P. Poggiolini, V. Curri, Proceedings of the ECOC 2005, Glasgow, UK, 2005106 (2005).

*Corresponding author: mehtab91singh@gmail.com